

1 Fuel reactor modelling in Chemical-Looping Combustion of coal:

2 1. Model formulation

3
4 Alberto Abad*, Pilar Gayán, Luis F. de Diego, Francisco García-Labiano, Juan Adánez
5 Instituto de Carboquímica (ICB-CSIC), Miguel Luesma Castán 4, 50018-Zaragoza, Spain

6
7 * Corresponding author: Tel.: +34 976 733 977; fax: +34 976 733 318.

8 E-mail addresses: abad@icb.csic.es, pgrayan@icb.csic.es, ldediego@icb.csic.es,
9 glabiano@icb.csic.es, jadanez@icb.csic.es

10

11 **Abstract**

12 A fundamental part of the reliability of the Chemical-Looping Combustion system when a
13 solid fuel, such as coal, is fed to the reactor is based on the behaviour of the fuel reactor,
14 which determines the conversion of the solid fuel. The objective of this work is to develop
15 a model describing the fuel reactor in the Chemical-Looping Combustion with coal
16 (CLCC) process. The model is used to simulate the performance of the 1 MW_{th} CLCC rig
17 built in the Technology University of Darmstadt. The fuel reactor is a fluidized bed
18 working at high velocity regime, using ilmenite as oxygen carrier. The developed model is
19 based on semi-empirical correlations, and considers the reactor fluid dynamics, the coal
20 conversion and the reaction of the oxygen carrier with evolved gases from coal. The
21 efficiency of a carbon separation system is also considered in order to analyze this
22 parameter on the fuel reactor performance.

1 The main outputs of the model are presented in this work, i.e. (1) the fluid dynamics
2 structure of the reactor; (2) the axial profiles of gas composition and flows (volatiles, CO,
3 H₂, CO₂ and H₂O); (3) the conversion of the oxygen carrier and char in the reactor; (4) the
4 char concentration in the reactor; (5) the gas composition and solids flow in the upper
5 reactor exit; and (6) the char flow to the air reactor. From these outputs the oxygen demand
6 of the flue gases and the CO₂ capture efficiency are calculated.
7 Simulations on the effect of the efficiency of the carbon separation system are presented. A
8 highly efficient carbon separation system should be used to reach a high carbon capture
9 value. Also incomplete combustion of gases is predicted in the fuel reactor, mainly from
10 unconverted volatile matter. The model can be later used to obtain basic design parameters
11 of the fuel reactor and optimize its operation.

12

13

14 **Keywords:** Combustion, Fluidization, Mathematical modelling, Simulation, Chemical-
15 Looping Combustion, Coal.

16

1 **1. Introduction**

2 Chemical-Looping Combustion (CLC) is one of the most promising technologies to carry
3 out the CO₂ capture at a low cost. CLC is based on the transfer of the oxygen from air to
4 the fuel by means of a solid oxygen carrier that circulates between two interconnected
5 fluidized beds: the fuel and the air reactors. In the fuel reactor the oxygen carrier is reduced
6 through oxidation of the fuel. The oxygen carrier is regenerated in the air reactor as the
7 inlet air flow reacts with the solids. The stream of combustion gases from the fuel reactor
8 contains primarily CO₂ and H₂O. Water can be easily separated by condensation and a
9 highly concentrated stream of CO₂ ready for sequestration is achieved. The CO₂ capture is
10 inherent to this process, as the air does not get mixed with the fuel, and no additional costs
11 or energy penalties for gas separation are required.

12 In the last years increasing interest is found about the application of CLC using coal as fuel,
13 regarding the intensive use of this fuel (Adánez et al., 2012). Important progress has been
14 made in continuous operation of CLC with coal (Adánez, 2012). Among them, different
15 iron based oxygen carriers were used in several CLC systems, being the fuel reactor
16 designed as a bubbling fluidized bed (Berguerand and Lyngfelt, 2008a, 2008b and 2009;
17 Cuadrat et al., 2011, 2012a and 2012b), spouted bed (Gu et al., 2011) or high velocity
18 fluidized bed (Markström et al., 2012). In all these cases, gasification of coal is an
19 intermediate step happening in the fuel reactor. In these studies, complete combustion of
20 gases was not reached in the fuel reactor, making necessary to take additional actions, as to
21 add a final gas polishing step with pure oxygen. Often the “oxygen demand” parameter, Ω_T ,
22 is used to describe the fraction of oxygen required in the oxygen polishing step. Besides,
23 high carbon capture can be accomplished by using high temperatures and/or implementing

1 a carbon separation system between the fuel and air reactors. The carbon separation system
2 is used to separate char particles from oxygen carrier and to return them to the fuel reactor,
3 diminishing the bypass of char particles into the air reactor.

4 A fundamental part of the reliability of a Chemical–Looping Combustion of Coal (CLCC)
5 system is based on the behaviour of the fuel reactor. This will determine the unburnt gas
6 losses obtained at the exit of the reactor and the remaining char in the stream of solids
7 going out from the fuel reactor. The modelling of the reactor would be helpful for the
8 design, optimization, and scale–up of the process, in order to obtain high coal conversion in
9 the fuel reactor of a CLCC system.

10 Some works have been presented in the literature for the modelling of the process involved
11 in the fuel reactor of a CLCC system. These models can be included in three general
12 groups: (1) simple models that does not considers the complex fluid dynamic existing in a
13 fluidized bed (Cuadrat et al., 2012c; Kramp et al., 2012; Ströhle et al., 2009 and 2010); (2)
14 macroscopic models based on empirical correlations for the fluid dynamic of a fluidized
15 bed (Brown et al., 2010; Schöny et al., 2011); and (3) multiphase computational fluid
16 dynamic (CFD) models (Mahalatkar et al., 2011).

17 Simple models consider a highly simplified description of the fuel reactor fluid dynamic,
18 but they do not include the complex distribution of gas and solids in a fluidized bed. Thus,
19 Cuadrat et al. (2012c) predicted the carbon capture and oxygen demand reached in a
20 bubbling fluidized bed with continuous feeding of coal and oxygen carrier. The difficulty
21 for gas in bubbles to reach the particles in the emulsion phase was considered with a
22 parameter for the contact efficiency between volatile matter and oxygen carrier particles.

23 Kramp et al. (2012) presented the effect on the carbon capture by using a carbon stripper as
24 carbon separation system. In this work, the fuel reactor was considered in perfect mixing

1 for solids and gas, and complete combustion of gases evolved in the fuel reactor was
2 assumed. A high-velocity fluidized bed was modelled as fuel reactor by Ströhle et al. (2009
3 and 2010). Both dense phase and lean phase were modelled as perfectly stirred reactors, the
4 second one after the first one.

5 In other cases, more elaborated models have been used. A two phase model was used by
6 Brown et al. (2010) to predict the carbon conversion in a batch fluidized bed with
7 continuous feeding of coal. The work done by Mahalatkar et al. (2011) presented
8 simulation and validation of the CFD model on a batch fluidized bed reactor. Schöny et al.
9 (2011) built an empirical model which considers the complex solids and gas flow in a high-
10 velocity fluidized bed. Schöny et al. (2011) focused their results in the combustion of gases
11 evolved in the fuel reactor, and point out the relevance of the coal particle size on the gas
12 conversion.

13 Nevertheless, model considering the complex fluid dynamics of a fluidized bed being able
14 to predict the behaviour regarding the carbon capture and combustion efficiency of a
15 continuously operated fuel reactor with solid fuels is not found in the literature.

16 In this work, a mathematical model for the fuel reactor of the 1 MW_{th} CLCC pilot rig
17 erected at TU Darmstadt is developed (Galloy et al., 2011). This reactor is a fluidized bed
18 working at high velocity regime. The process carried out in the reactor is the coal
19 combustion using ilmenite as oxygen carrier. The model considers the complex fluid
20 dynamics of a circulating fluidized bed, the coal conversion, i.e. coal pyrolysis and char
21 gasification, and the rate of the oxygen carrier reduction by gaseous compounds. The model
22 is able to predict the carbon capture and combustion efficiency of the CLCC system.

23

1 **2. Fuel reactor model**

2 The model developed is focused on the fuel reactor behaviour, being a fluidized-bed
3 reactor working at the high-velocity regime. The reactor is based on the design of a 1 MW_{th}
4 CLCC unit at TU Darmstadt (Abdulally et al., 2012). A diagram of this reactor is presented
5 in Fig. 1. The coal stream is physically mixed with the oxygen carrier in the fuel reactor
6 and the oxygen carrier reacts with the gas products from coal pyrolysis and gasification.
7 The stream of combustion gases from the fuel reactor contains primarily CO₂ and H₂O,
8 together with some unburnt compounds (CO, H₂, hydrocarbons -C_xH_y-). At the high-
9 velocity regime, a fraction of the particles having reached the exit duct height follows the
10 gas stream towards the two step cyclone system, where solid particles are separated. The
11 cyclone system is composed by: (1) a low-efficiency cyclone where mostly oxygen carrier
12 particles are separated; and (2) and a high-efficiency cyclone which separates char particles
13 not recovered by the low-efficiency cyclone, which are recirculated to the fuel reactor.
14 The solids stream separated by the low-efficiency cyclone consists of oxygen carrier mixed
15 with a small fraction of char. It is desirable that the solids flow recovered by the cyclone
16 was higher than the solids circulation flow rate to the air reactor. Thus, a fraction of the
17 solids exiting the cyclone are externally recirculated to the bottom part of the reactor. The
18 other fraction of solids is introduced to a carbon stripper unit in order to improve the carbon
19 separation before oxygen carrier entering to the air reactor. Carbon separated in the carbon
20 stripper is sent back to the fuel reactor. Thus, the cyclone system and the carbon stripper act
21 together as a carbon separation system.

22 The flow of char in the solids stream to the air reactor depends on the efficiency of
23 separation of the carbon separation system. The processes happening in the components of
24 the carbon separation system, i.e. cyclones + carbon stripper, are not modelled in this work,

1 but the whole efficiency of char removal is considered in the model to simulate the
2 performance of the fuel reactor.

3 In this work a macroscopic model is developed, which is based on empirical and semi-
4 empirical expressions. The model considers the fluid dynamics of the fuel reactor in the
5 high-velocity fluidized bed regime, as well as the mixing of gas and solid particles in the
6 reactor. The mixing of gas and solid particles influences the performance of a fluidized-bed
7 reactor; a high mixing rate contributes to an effective distribution of reactants, whereas an
8 insufficient mixing can lead to uncompleted reaction. Therefore, an adequate understanding
9 of the mixing behaviour is important to predict the performance of the reactor.

10 The modelling of the high-velocity fluidized-bed reactor is divided in two fields: fluid
11 dynamics and mass balances. At this point, it is remarkable that the gas velocity, u_g , is not
12 constant with the reactor height. The gas velocity increases by the gas entering together
13 with the char from the carbon stripper, the gases from the pyrolysis of coal, the gas
14 generated during char gasification, the gas expansion during the conversion of
15 hydrocarbons in the volatile matter and the gas expansion due to the pressure drop in the
16 reactor. This affects the fluid dynamics of the fluidized bed. As the increase in gas velocity
17 depends on the reaction rate of gases with the oxygen carrier and char, fluid dynamics and
18 mass balances in the reactor must be solved simultaneously. In mass balances the kinetics
19 of char gasification and oxygen carrier reaction with gaseous products, i.e. H_2 , CO and
20 CH_4 , are included.

21

22 *2.1. Fluid dynamics of the fuel reactor*

23 The fuel reactor is considered to be in the high-velocity fluidisation regime. The model is
24 based on the fluid dynamics modelling presented by Pallarès and Johnsson (2006), which

1 considers the gas and solids flows inside the reactor and the gas–solids mixing patterns in
2 the different regions in which it can be divided. This model was based on studies especially
3 devoted to large scale circulating fluidized beds, and gives a simple and complete model of
4 the circulating loop fluid dynamics. This model was successfully used to predict the
5 behaviour of a 12 MW_{th} CFB unit (Adánez et al., 2003).

6 In the model, the reactor is divided into two vertical zones with respect to axial
7 concentration and backmixing of solids, see Fig. 2: 1) a bottom bed with a high and roughly
8 constant solids concentration; and 2) a freeboard above the bottom bed, where there is a
9 pronounced decay in solids concentration with height. The model can be considered as 1.5
10 dimensional, with the main dimension the axial direction, but takes into account lateral
11 exchange of solids in the freeboard between the core and an annulus close to the reactor
12 wall. Moreover, gas distribution and mixing between the emulsion and bubble in the
13 bottom bed is considered. Thus, the gas flow in the bottom bed is shared between the
14 emulsion and bubble phases, with gas mixing between them. Solids are in the emulsion
15 phase, where gas flow maintains the minimum fluidizing conditions; whereas the rest of gas
16 goes through bubbles, where there are not solids.

17 The freeboard is composed by the splash or cluster phase and a transport or dispersed
18 phase. Both the splash and transport phases are superimposed but with different mixing
19 behaviour. The splash phase has a strong solids backmixing with solids in the bottom bed.

20 The transport phase is characterized by a core/annulus flow structure. A net flow up of
21 solids goes through the core, F_c , and solids backmixing occurs at the reactor walls, F_w .

22 The presence of three fluid dynamically different zones implies that they should be
23 investigated separately with respect to gas mixing.

1 The hypotheses considered for the fluid dynamic model are: (1) steady state; (2) isothermal
2 bed at macroscopic level; (3) perfect mixing of the solids in the bottom bed and splash
3 phase; (4) plug flow of gas in all zones of the reactor but lateral exchange of gas between
4 bubbles and emulsion in the bottom bed; (5) gas stagnant in the annulus is considered, that
5 is, the gas flows only through the core; (6) plug flow up of solids through the core in the
6 transport phase with lateral flow of solids from the core to the annulus; and (7) no existence
7 of particle fragmentation or attrition.

8

9 *2.1.1. Fluid dynamics in the bottom bed*

10 The bottom bed is defined as the zone located at the bottom of the bed characterized by a
11 roughly constant solids concentration. The gas flow in the bottom bed is considered by a
12 modified two phase flow as proposed by Johnsson et al. (1991). The total gas flow is
13 expressed in terms of gas velocity considering the whole reactor section as: (1) the flow in
14 the particulate or emulsion phase at the minimum fluidization velocity, $(1-\delta_b)u_{mf}$; (2) the
15 visible bubble flow, u_{vis} , related to the gas in the bubbles at the rising velocity of the
16 bubbles; and (3) the gas throughflow, u_{tf} , corresponding to the excess of inlet gas over the
17 gas in the emulsion and bubbles. The gas throughflow can be understood as a stream of gas
18 passing through bubbles. Thus, in terms of superficial gas velocities the total gas flow, u_g ,
19 is divided following the equation

$$20 \quad u_g = (1 - \delta_b)u_{mf} + u_{vis} + u_{tf} \quad (1)$$

21 δ_b being the volumetric fraction of bubbles in the bottom bed.

22 A gas exchange between bubbles (u_{vis} and u_{tf}) and emulsion (u_{mf}) is considered allowing the
23 exchange of products and reactants between these phases. The model assumes that the

1 emulsion phase remains under minimum fluidization condition. Thus, the flow in excess
 2 over the minimum gas velocity, u_{mf} , is shared between the visible gas in the rising bubbles,
 3 u_{vis} , and the throughflow, u_{tf} . The minimum fluidization velocity, u_{mf} , is calculated using
 4 the correlation proposed by Wen and Yu (1966)

$$5 \quad \text{Re}_{p,mf} = \frac{u_{mf} \rho_g d_p}{\mu_g} = \sqrt{C_1^2 + C_2 \text{Ar}} - C_1 \quad (2)$$

6 The values for $C_1 = 27.2$ and $C_2 = 0.0408$ suggested by Grace (1986) are used. The porosity
 7 at the minimum fluidization conditions, ϵ_{mf} , is calculated with the expression proposed by
 8 Broadhurst and Becker (1975):

$$9 \quad \epsilon_{mf} = 0.586 \phi^{-0.72} \text{Ar}^{-0.029} \left(\frac{\rho_g}{\rho_s} \right)^{0.021} \quad (3)$$

10 The presence of bubbles gives an additional expansion of the bed compared to the
 11 minimum fluidization conditions. For a high-velocity fluidized bed, two fluidization
 12 regimes were considered depending on the gas velocity. At low velocities, a modified
 13 model developed for a stationary fluidized bed can be used (Johnsson et al., 1991). The
 14 visible bubble flow and the throughflow are written:

$$15 \quad u_{vis} = \Psi (u_g - u_{mf} (1 - \delta_b)) \quad (4)$$

$$16 \quad u_{tf} = (1 - \Psi) (u_g - u_{mf} (1 - \delta_b)) \quad (5)$$

17 Ψ being the ratio of the visible bubble flow, u_{vis} , to the total flow through the bubbles, $u_{vis} +$
 18 u_{tf} , and it is calculated as

$$19 \quad \Psi = f_b \left(z + 4\sqrt{A_0} \right)^{0.4} \quad (6)$$

20 The parameter A_0 is the gas-distributor area per nozzle. The function f_b is calculated from
 21 the following equation:

$$f_b = \frac{0.26 + 0.70e^{-3300d_p}}{(0.15 + u_g - u_{mf})^{1/3}} \quad (7)$$

The bubble fraction in the bottom bed is:

$$\delta_b = \frac{u_{vis}}{u_{vis} + u_{b\infty}} \quad (8)$$

With the assumption of the minimum fluidization porosity in the emulsion phase, the single bubble velocity, $u_{b\infty}$, is

$$u_{b\infty} = 0.71\sqrt{gd_b} \quad (9)$$

the bubble size being calculated with the correlation by Darton et al. (1977):

$$d_b = 0.54(u_g - u_{mf})^{0.4} (z + 4\sqrt{A_0})^{0.8} g^{-0.2} \quad (10)$$

Once obtained the fraction of bubbles in the bed, δ_b , the average bed porosity at a fixed position in the bottom bed can be obtained as:

$$\varepsilon_b = (1 - \delta_b)\varepsilon_{mf} + \delta_b \quad (11)$$

At high velocities, the average bed voidage levels out. In this regime, bubbles are of an exploding type, providing a large and almost free passage of gas through the bottom bed during the time of bubble eruption. Thus, an increase in the gas velocity in the bottom bed does not produce a further increase in the voidage because the excess of gas is used to increase the throughflow. The porosity at the bottom bed is constant and equal to the saturation porosity, calculated as:

$$\varepsilon_{b,sat} = 0.5452 + \frac{495.5}{\Delta P_0} + \frac{4.9 \cdot 10^{-6}}{d_p} \quad (12)$$

1 At this regime, the porosity obtained using Eq. (11) is higher than $\varepsilon_{b,sat}$. In this case, the
 2 porosity of the bed is taken to be equal to the saturation porosity, $\varepsilon_b = \varepsilon_{b,sat}$. The bubble
 3 fraction, δ_b , becomes the value obtained at saturation condition, $\delta_{b,sat}$

$$4 \quad \delta_b = \delta_{b,sat} = \frac{\varepsilon_{b,sat} - \varepsilon_{mf}}{1 - \varepsilon_{mf}} \quad (13)$$

5 The visible bubble flow and the throughflow are obtained as:

$$6 \quad u_{vis} = u_{vis,sat} = \frac{\delta_{b,sat}}{1 - \delta_{b,sat}} u_{b\infty} \quad (14)$$

$$7 \quad u_{tf} = u_g - u_{vis} - u_{mf} (1 - \delta_b) \quad (15)$$

8 and the share between u_{vis} and u_{tf} , given by the dimensionless visible bubble flow, Ψ_{sat} , is:

$$9 \quad \Psi = \Psi_{sat} = \frac{u_{vis}}{u_g - u_{mf} (1 - \delta_{b,sat})} \quad (16)$$

10

11 *2.1.2. Fluid dynamics in the freeboard*

12 The freeboard starts from the upper limit of the bottom bed, and it is characterized by a
 13 decrease in the solids concentration with the reactor height. The solids suspension in the
 14 freeboard is divided into two phases, a splash phase and a transport phase, each one with
 15 different fluid dynamical behaviour. The backmixing behaviour is different in each of these
 16 zones. The splash phase is characterised by a strong backmixing of solids with the bottom
 17 bed and it is composed by clusters of solids projected from the bottom bed due to the
 18 eruption of bubbles. Instead, the transport phase is characterised by a more disperse zone.
 19 The transport phase has a core-annulus structure, where there is a net flux of solids upwards
 20 in the core, and downwards in the annulus. Thus, the backmixing in the transport phase
 21 occurs mainly at the reactor walls.

1 The gas flows up through the core, whereas it is assumed to be stagnant in the annulus, near
2 the walls of the reactor. The thickness of the annulus zone increases downwards along the
3 reactor from the exit zone, where it is considered to be zero. The thickness of the annulus
4 zone becomes:

$$5 \quad \delta_w = 0.01076(H_r - z) \quad (17)$$

6 The thickness of the annulus grows downwards until it reaches a saturation value, which is
7 obtained from the following equation:

$$8 \quad \delta_{w,sat} = 0.06456d_{react} \quad (18)$$

9 The height from the bottom of the reactor at which the saturation value is reached is:

$$10 \quad z_{sat} = H_r - 6d_{react} \quad (19)$$

11 Therefore, the cross section through which the gas is flowing, A_c , increases above z_{sat} ,
12 affecting the gas velocity in the freeboard, u_g .

13 In the model developed, the splash and transport phases start from the upper limit of the
14 bottom bed. Both phases present a decrease in the solids concentration with the reactor
15 height, but this decrease is stronger for the splash phase. The splash phase is dominating the
16 solids suspension in the lower part of the freeboard and the transport phase prevails in the
17 upper part if flow is completely developed.

18 The decay in solids concentration of the splash phase is given by the decay factor a :

$$19 \quad \frac{dC_{spl}}{dz} = -aC_{spl} \quad (20)$$

20 The decay factor, a , depends on the superficial gas velocity and the terminal velocity of the
21 particles, and it is calculated as

$$22 \quad a = 4 \frac{u_t}{u_g} \quad (21)$$

1 Concerning the transport phase, the solids concentration in the core is assumed to follow
 2 the expression:

$$3 \quad \frac{dC_{tr,i}}{dz} = -K_i C_{tr,i} \quad (22)$$

4 the decay factor K_i being calculated as:

$$5 \quad K_i = \frac{0.23}{u_g - u_{t,i}} \quad (23)$$

6 Both decay factors a and K are not constant along the freeboard, because the cross section
 7 of the core, A_c , and the gas velocity, u_g , change with the height in the reactor.

8 Note that the concentration of oxygen carrier and char in the transport phase was calculated
 9 separately by Eqs. (22-23), being $C_{tr,i}$ the concentration of the solids i considered, i.e.

10 oxygen carrier or char particles. The solids concentration in the transport phase is taken
 11 from the flow rate of entrained solids from the bottom region, $F_{0,i}$:

$$12 \quad C_{tr,i,H_b} = \frac{F_{0,i}}{A_{c,H_b} (u_{g,H_b} - u_{t,i})} \quad (24)$$

13 where the flow rate of solids $F_{0,i}$ is obtained using the equation given by de Diego et al.
 14 (1995):

$$15 \quad F_{0,i} = 131.1 \left[\frac{A_c u_g}{\epsilon_b} \rho_g \left(\frac{Re_{s,i}}{Ar_i} \right)^{0.31} \right]_{H_b} \quad (25)$$

16 A simple correlation proposed by Haider and Levenspiel (1989) was used to calculate the
 17 terminal velocity:

$$18 \quad u_{t,i} = u_{t,i}^* \left(\frac{\rho_g^2}{\mu_g (\rho_i - \rho_g) g} \right)^{-1/3} \quad \text{being} \quad u_{t,i}^* = \left(\frac{18}{Ar_i^{2/3}} + \frac{2.335 - 1.744\phi_i}{Ar_i^{1/6}} \right)^{-1} \quad (26)$$

1 The initial condition to solve these equations is taken following a continuity expression for
 2 the solids concentration at the upper bottom bed height, H_b :

$$3 \quad C_{spl,H_b} = C_{b,H_b} - C_{tr,H_b} \quad (27)$$

4 being the total concentration in the transport phase the sum of the concentration of char and
 5 oxygen carrier particles

$$6 \quad C_{tr,H_b} = C_{tr,OC,H_b} + C_{tr,C,H_b} \quad (28)$$

7 The total solids concentration in the freeboard was the sum of the solids in the splash and
 8 the transport phases:

$$9 \quad C_{f\dot{b}} = C_{spl} + C_{tr} \quad (29)$$

10 Particles in the splash phase are being in perfect mixing with the bottom bed. Instead, the
 11 transport or dispersed phase presents a net upward flow. Particles entrained up through the
 12 transport region can be separated to the annulus near the reactor wall, where particles are
 13 internally recirculated to the bottom bed, or externally sent to the cyclone after having
 14 reached the exit duct height. From the solids concentration in the core, the upwards flow of
 15 solids i , $F_{c,i}$, can be obtained as:

$$16 \quad F_{c,i} = C_{tr,i} A_c (u_g - u_{t,i}) \quad (30)$$

17 The transport phase is assumed to be the only solid phase contributing to the externally
 18 recirculated flow of solids i , $F_{s,i}$, which can be obtained from the solid flow at the exit zone,
 19 $(F_{c,i})_{H_r}$, and the backflow ratio, $k_{b,i}$, for every solid i , i.e. oxygen carrier or char particles:

$$20 \quad k_{b,i} = \frac{(F_{w,i})_{H_r}}{F_{s,i}} = \frac{(F_{c,i})_{H_r} - F_{s,i}}{F_{s,i}} \quad (31)$$

1 The total flow of solids from the fuel reactor is the sum of the flow of oxygen carrier and
 2 char.

$$3 \quad F_s = F_{s,OC} + F_{s,char} \quad (32)$$

4 During the discretisation carried out to solve the solids profiles, the lateral diffusion of
 5 particles i , $F_{t,i}$, corresponding with the solids net flow from the core to the annulus in the
 6 node j is obtained from the difference on the solids flow upwards by the core in the node j
 7 and $j+1$:

$$8 \quad F_{t,i} \Big|_j = F_{c,i} \Big|_j - F_{c,i} \Big|_{j+1} \quad (33)$$

9 Thus, profiles of the solids down flow by the annulus can be estimated as:

$$10 \quad F_{w,i} \Big|_j = F_{w,i} \Big|_{j+1} + F_{t,i} \Big|_j \quad (34)$$

11 with initial value at the reactor exit, $(F_{w,i})_{H_r}$, obtained from Eq. (31). Thus, the solids
 12 concentration in the annulus can be obtained at every position z :

$$13 \quad C_{w,i}(z) = \frac{F_{w,i}(z)}{A_w(z)u_{t,i}} \quad (35)$$

14 Despite its importance, little information is available on the magnitude of the backflow
 15 ratio, k_b (Harris et al., 2003; Johnsson et al., 1999). Factors as the presence of internals near
 16 the exit zone, the inlet area of the cyclone, the slip velocity or the value of the solids net
 17 flow can affect this parameter. Pallarès and Johnsson (2006) reviewed the effect of the
 18 particle slip velocity on the particle entrainment probability, which in turn affects to the
 19 backflow ratio. They showed that at high particle slip velocity, the particle entrainment
 20 probability varies between 0.6 and 1. Taken an average value for the particle entrainment
 21 probability of 0.8, a value of k_b about 0.2 was calculated, which was taken as a reference
 22 value in this work.

1 Finally, the mixing gas behaviour in the freeboard has been considered. This phenomenon
 2 is taken into account by the use of a contact efficiency parameter, ξ_{g-s} , between gas and
 3 solids in the freeboard, calculated by the equation proposed by Furusaki et al. (1976)

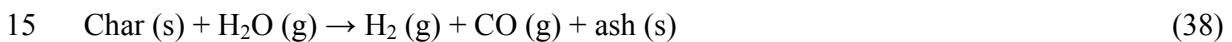
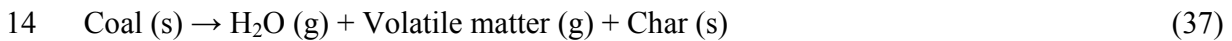
$$4 \quad \xi_{g-s}(z) = 1 - 0.75 \left(\frac{C_{frib}(z)}{C_b(z = H_b)} \right)^{0.4} \quad (36)$$

5 C_{frib} being the solids concentration in the freeboard given by Eq. (29) and C_b the solids
 6 concentration calculated in the upper limit of the bottom bed. The contact efficiency
 7 parameter is applied on the reaction rate calculated at each axial position into the freeboard.

8

9 *2.2. Mass balances into the reactor*

10 Mass balances for the different reacting compounds and products are developed for the
 11 phases in the bottom bed and the freeboard. The pathway for coal conversion with the
 12 oxygen carrier is considered to happen in two steps. First drying, pyrolysis and gasification
 13 to produce gaseous compounds:



17 The initial moisture of coal is evaporated, and steam is generated. CO, H₂ and CH₄ are
 18 uniquely considered as reducing gases in the mass balances (Cuadrat et al., 2012c). In the
 19 second step, the gaseous compounds react with the oxygen carrier particles towards CO₂
 20 and H₂O following the pathway showed by Eqs. (40)–(42).





2 The pathway for reaction of methane with the oxygen carrier considers that H₂O is a
3 primary product during the reaction with the metal oxide (Dewaele and Froment, 1999).

4 Thus, the CH₄ conversion was considered to happen in two steps: first towards CO and
5 H₂O and later CO reacts towards CO₂.

6 Moreover, the model can assume, or not, that the reaction products (CO, H₂, CO₂ and H₂O)
7 reach instantaneously the water–gas shift (WGS) equilibrium –Eq. (43)– in all phases of the
8 reactor.



10

11 *2.2.1. Mass balances in the bottom bed*

12 In the bottom bed, a gas exchange between bubbles (u_{vis} and u_{tr}) and emulsion (u_{mf}) is
13 considered allowing the exchange of products and reactants between these phases by
14 diffusive and/or bulk flow mechanism. Indeed, as the gas suffers a volumetric expansion
15 during the char gasification and conversion of hydrocarbons, some of the gas in the
16 emulsion must move to the bubble phase to maintain the minimum fluidization condition in
17 the emulsion phase. Considering all the above assumptions, the mass balances were given
18 by the following differential equations for each gas i (CO, H₂, CO₂, H₂O and CH₄) in the
19 emulsion and bubble phases, respectively:

$$20 \quad \frac{dF_{e,i}}{dV} = \frac{d[(1-\delta_b)u_{mf}C_{e,i}]}{dz} =$$

$$-(1-\delta_b)\left[\sum(-\bar{r}_{g,i})_{OC} + \sum(-\bar{r}_{g,i})_{char}\right]_e - \delta_b k_{be}(C_{e,i} - C_{b,i}) - y_{e,i} \frac{dF_{exc}}{dV} - \frac{dF_{WGS,i}}{dV} \quad (44)$$

$$21 \quad \frac{dF_{b,i}}{dV} = \frac{d[(u_{vis} + u_{tr})C_{b,i}]}{dz} = \delta_b k_{be}(C_{e,i} - C_{b,i}) + y_{e,i} \frac{dF_{exc}}{dV} - \frac{dF_{WGS,i}}{dV} \quad (45)$$

1 The first term in the right side on Eq. (44) represents the amount of gas i consumed or
2 generated in the differential volume element dV . $\sum(-\bar{r}_{g,i})_{OC}$ is the net consumption or
3 generation rate of the gas i by reaction with the oxygen carrier in the emulsion phase
4 following the scheme given in Eqs. (40)–(42). $\sum(-\bar{r}_{g,i})_{char}$ is the net consumption or
5 generation of the gas i by the char gasification, given by Eqs. (38) and (39). The second
6 term is the net gas amount of gas i flowing from the emulsion to the bubble by gas
7 diffusion. The third term refers to the excess of gas in the emulsion that moves to the
8 bubbles because of the gas expansion produced in the differential volume. Finally, the
9 fourth term is the amount of gas i reacted to fulfil the WGS equilibrium. Similar
10 descriptions can be done for the mass balance in the bubble phase, see Eq. (45), excepting
11 that in this phase there is not gas–solid reaction. These equations allow determining the
12 concentration of gas i in both phases: emulsion and bubbles. The bubble–emulsion gas
13 exchange coefficient, k_{be} , is obtained using the correlation given by Foka et al. (1996) for
14 turbulent fluidized beds:

$$15 \quad k_{be} = 1.631 u_g \text{Sc}^{0.37} \quad (46)$$

16

17 2.2.2. Mass balances in the freeboard

18 In the freeboard, the mass balance for each gas in a differential element of bed yields

$$19 \quad \frac{dF_{dil,i}}{dV} = \frac{d[u_g C_{dil,i}]}{dz} = \quad (47)$$

$$- \left[\xi_{g-s} \sum(-\bar{r}_{g,i})_{OC} + \sum(-\bar{r}_{g,i})_{char} \right]_{spl} - \left[\xi_{g-s} \sum(-\bar{r}_{g,i})_{OC} + \sum(-\bar{r}_{g,i})_{char} \right]_{tr} - \frac{dF_{WGS,i}}{dV}$$

20 The first and second terms in the right side on Eq. (47) represent the amount of gas i
21 consumed or generated in the differential volume element, dV , by reaction of gases with the

1 oxygen carrier and char particles in the splash phase and in the transport phase,
 2 respectively. ξ_{g-s} is the contact efficiency between gas and solids in the freeboard given by
 3 Eq. (36). The last term is the amount of gas i reacted to fulfil the WGS equilibrium.
 4 Different behaviour for the solids is assumed for the splash and the transport phases. Solids
 5 into the splash phase are in perfect mixing with the bottom bed, whereas solids in the
 6 transport phase have a net flow upwards through the core. The average conversion for the
 7 splash phase corresponds to the same as solids conversion existing in the bottom bed. The
 8 solids conversion in the transport phase is a function of the axial location, and it increases
 9 as the solids flow up through the core. The variation of the solids conversion, as much as
 10 for oxygen carrier as for char particles, is calculated using the following equation:

$$11 \quad \frac{dX_i}{dz} = \frac{dX_i}{dt} \frac{dt}{dz} = \frac{dX_i}{dt} \frac{1}{u_{s,i}} \quad (48)$$

12 $u_{s,c}$ being the velocity of solids in the core

$$13 \quad u_{s,i} = u_g - u_{t,i} \quad (49)$$

14

15 2.2.3. Boundary and initial conditions

16 The boundary conditions to solve the above mass balances are the following:

17 a) At the bottom of the bed, the gas flow of each compound i is the flow at the reactor inlet.

$$18 \quad F_i|_{z=0} = F_{i,in} \quad (50)$$

19 b) At the feeding point of coal, H_{coal} , the flow of the gas i in the volatile matter, $F_{i,vm}$, is
 20 instantaneously evolved to the gas phase. If the feeding point is inside the bottom bed,
 21 the volatiles flow is joined to the bubbles flow.

$$22 \quad F_i|_{z=z_{coal}} = F_i + F_{i,vm} \quad (51)$$

1 c) The gas flow coming together with the recirculated char from the carbon stripper, $F_{i,CS}$,
 2 is added to the gas flow in the reactor at the height of the char feeding point, H_{CS} . If H_{CS}
 3 is inside the bottom bed, the gas flow is joined to the bubbles flow.

$$4 \quad F_i|_{z=z_{CS}} = F_i + F_{i,CS} \quad (52)$$

5 Moreover, the following initial conditions should be fulfilled:

6 a) The amount of solids in the fuel reactor should be that required to give the pressure drop
 7 initially assumed. Thus, the height of the bottom bed is calculated to fulfil the amount of
 8 solids required.

$$9 \quad \Delta P = \int_0^{H_b} C_b \rho_s g dz + \int_{H_b}^{H_r} C_{dil} \rho_s g dz \quad (53)$$

10 b) The oxygen supplied by the oxygen carrier must be equal to the oxygen reacted with the
 11 reacting gases from coal pyrolysis and gasification:

$$12 \quad F_{OC} R_{OC} \Delta X_{OC} = M_O \left\{ (F_{H_2O} + 2F_{CO_2} + F_{CO})_{out} - (F_{H_2O} + 2F_{CO_2} + F_{CO})_{in} \right\} \quad (54)$$

13 F_{OC} being the circulation flow rate of the oxygen carrier between air and fuel reactors,
 14 and ΔX_{OC} the variation of the mean conversion of solids in the reactor.

$$15 \quad \Delta X_{OC} = \bar{X}_{OC,out} - \bar{X}_{OC,in} \quad (55)$$

16 c) The carbon in the char flowing to the air reactor from the carbon stripper, $F_{C,AR}$, must be
 17 equal to the ungasified carbon from the coal in the fuel reactor.

$$18 \quad F_{C,AR} = \frac{[C]_{coal} \cdot F_{coal}}{M_C} - \left[(F_{CO_2} + F_{CO} + F_{CH_4})_{out} - (F_{CO_2})_{in} \right] \quad (56)$$

19 The carbon flowing to the air reactor from the carbon stripper can be also calculated as a
 20 function of the separation efficiency of the carbon separation system, η_{CCS} :

$$21 \quad F_{C,AR} = (1 - \eta_{CCS}) F_{C,FR} \quad (57)$$

1 In this calculation, it is considered that there is a fraction of char intrinsically returned to
 2 the fuel reactor, corresponding to the excess of solids flow exiting the fuel reactor
 3 regarding the recirculated solids flow, F_{OC} . Thus, $F_{C,FR}$ depends on the char flow going
 4 to cyclone, $F_{s,char}$, the ratio between the recirculated flow and solids flow going to the
 5 cyclone system, and the content of carbon in the reacted char, which depends on the
 6 initial carbon content in char and the char conversion.

$$7 \quad F_{C,FR} = \frac{F_{s,char}}{M_C} \frac{F_{OC}}{F_{s,OC}} \frac{(1 - X_{char})[C]_{fix}}{(1 - X_{char})[C]_{fix} + [ash]} \quad (58)$$

8 The char conversion, X_{char} , can be calculated as,

$$9 \quad X_{Char} = \frac{M_C F_{C,gasif}}{[C]_{fix} \cdot F_{coal}} = \frac{[C]_{fix} \cdot F_{coal} - M_C F_{C,AR}}{[C]_{fix} \cdot F_{coal}} \quad (59)$$

10 $F_{C,gasif}$ being the carbon gasified in the fuel reactor, calculated as:

$$11 \quad F_{C,gasif} = \int_0^{H_b} (1 - \delta_b) \left[\left(-\bar{r}_{g,H_2O} \right)_{char} + \left(-\bar{r}_{g,CO_2} \right)_{char} \right]_e S_{react} dz -$$

$$12 \quad \int_{H_b}^{H_r} \left[\left(-\bar{r}_{g,H_2O} \right)_{char} + \left(-\bar{r}_{g,CO_2} \right)_{char} \right]_{spl} S_{react} dz -$$

$$13 \quad \int_{H_b}^{H_r} \left[\left(-\bar{r}_{g,H_2O} \right)_{char} + \left(-\bar{r}_{g,CO_2} \right)_{char} \right]_{tr} S_{react} dz \quad (60)$$

12

13 2.3. Inputs to the model

14 The present study focuses on the fuel reactor of the 1 MW_{th} CLCC test plant at TU
 15 Darmstadt (Ströhle et al., 2010; Abdulally et al., 2012). The main inputs to the model are
 16 shown in Tables 1-6. The dimensions and main process parameters of this reactor are
 17 summarized in Tables 1 and 2. The main physical and chemical properties of solids are
 18 summarized in Tables 3-6, including the kinetic parameters for reduction of ilmenite and
 19 char gasification.

1 The solids circulation rate is selected to operate at an oxygen carrier to fuel ratio of $\phi = 1.2$.
 2 This value was selected according to the results showed by Cuadrat et al. (2012a), where
 3 the carbon capture increased as the ϕ ratio decreased. The oxygen carrier to fuel ratio, ϕ ,
 4 was defined as the availability of oxygen in the flow of oxygen carrier divided by the
 5 oxygen required to fully convert the fuel to CO₂ and H₂O:

$$6 \quad \phi = \frac{R_{O,ilm} F_{OC}}{\Omega_{coal}} \quad (61)$$

7 So, $\phi = 1$ corresponds to the stoichiometric flow of oxygen carrier needed for a full
 8 conversion of the fuel to CO₂ and H₂O. The oxygen demanded by coal is defined as:

$$9 \quad \Omega_{coal} = M_O (2[C]_{coal} / M_C + 0.5[H]_{coal} / M_H - [O]_{coal} / M_O) \cdot \dot{m}_{coal} \quad (62)$$

10 $[C]_{coal}$, $[H]_{coal}$ and $[O]_{coal}$ being the carbon, hydrogen and oxygen fractions in the fuel, whose
 11 values are obtained from the proximate analysis.

12

13 2.3.1. Oxygen carrier

14 Ilmenite has been widely studied as oxygen carrier in the CLCC process. Tests in units
 15 from 0.5 to 100 kW_{th} showed the good performance of this material in the process
 16 (Berguerand and Lyngfelt, 2008a, 2008b and 2009; Cuadrat et al., 2011, 2012a and 2012b;
 17 Markström et al., 2012). Ilmenite showed and increase in its reactivity through redox cycles
 18 during the so-called activation process (Adánez et al., 2010). A fast activation was observed
 19 in continuous operation in a 0.5 kW_{th} unit, whereas the oxygen transport capacity was
 20 maintained roughly constant (Cuadrat et al., 2011). In this work, activated ilmenite was
 21 considered as the oxygen carrier material for coal combustion. The physical properties of
 22 the activated ilmenite particles are shown in Table 3.

1 The kinetic parameters for the reduction of activated ilmenite with CH₄, H₂ and CO are in
 2 Table 4. These kinetic parameters were obtained in a previous work (Abad et al., 2011).
 3 The grain model with uniform reaction in the particle with changing grain size model in the
 4 grains was used to determine the reaction rate of the oxygen carrier particles. Every grain
 5 react following the shrinking core model (SCM) controlled by chemical reaction. The
 6 equations that describe the reaction rate are the following:

$$7 \quad \frac{dX_{OC,i}}{dt} = \left[\frac{3}{\tau_i} (1 - X_{OC,i})^{2/3} \right] \left[\frac{R_{OC,0}}{R_{OC}} \right] \quad \tau_i = \frac{\rho_m r_g}{b_i k_{OC,i} C_{p,i}^{n_i}} \quad (63)$$

8 $R_{OC,0}$ and R_{OC} being the oxygen transport capacity of ilmenite particles used for kinetic
 9 determination and of ilmenite particles considered in this work. Thus, $R_{OC,0} = 3.3$ wt.% and
 10 $R_{OC} = 4.0$ wt.% (Abad et al., 2011). The kinetic constant, $k_{OC,i}$, was calculated as a function
 11 of temperature:

$$12 \quad k_{OC,i} = k_{0,OC,i} e^{-E_{OC,i}/R_g T} \quad (64)$$

13 The average reaction rate of every reducing gas at each height in the reactor, $(-\bar{r}_{g,i})_{OC}$, was
 14 calculated from the average reaction rate of solids following the scheme given by Eqs.
 15 (40)–(42):

$$16 \quad (-\bar{r}_{g,i})_{OC} = \frac{(-\bar{r}_{OC,i})}{2d_i} \quad (65)$$

17 d_i being the stoichiometric coefficient for the combustion of the reacting gas i (CO, H₂ or
 18 CH₄) with molecular oxygen. The oxidation of CH₄ to CO and H₂O was considered in the
 19 mass balances, so $d_{CH_4} = 3/2$ was used for methane. In this sense, the stoichiometric factor
 20 b_{CH_4} used in the kinetic model (see Eq. (63)) also corresponds to the oxidation of CH₄ to

1 CO and H₂O, i.e. $b_{CH_4} = 4.34$ (see Table 4), similarly to the modification done by Abad et
 2 al. (2010).

3 To obtain the average reaction rate of the oxygen carrier, $(-\bar{r}_{OC,i})$, the residence time
 4 distribution of the solids, $E(t)$, is taken into account. So, the average reaction rates of the
 5 oxygen carrier in a determined position in the reactor can be obtained as

$$6 \quad (-\bar{r}_{OC,i}) = \frac{\rho_{OC} R_{OC}}{M_O} (1 - \varepsilon_z) \int_0^{t_{r,i}} \left[\frac{d(X_{OC}(t) - \bar{X}_{OC,in})}{dt} \right]_i E(t) dt \quad (66)$$

7 Assuming a perfect mixing of the solids in the bottom bed and the splash regions, the
 8 residence time distribution curve of the solids, $E(t)$, is given by the following equation
 9 (Levenspiel, 1981):

$$10 \quad E(t) = \frac{1}{t_{mr}} e^{-t/t_{mr}} \quad (67)$$

11 where t_{mr} is the mean residence time of particles in the whole reacting zone of the
 12 fluidized-bed reactor.

13 Eq. (66) has been expressed to consider that the oxygen carrier can be introduced into the
 14 reactor with a mean conversion of the oxygen carrier for the reduction reaction, $\bar{X}_{OC,in}$,

15 higher than 0, i.e. particles could not have been fully oxidized in the air reactor. It is
 16 assumed that the oxidized compound in the grains is in the outer part, being the inner core
 17 the material not oxidized. Therefore, the reduction proceeds from the outer surface of the
 18 grain towards the interior of the grain following the SCM (Abad et al., 2007; García-
 19 Labiano et al., 2004). Thus, the values of $t_{r,i}$ are defined as the reacting time of an oxygen
 20 carrier particle from zero conversion until the maximum variation possible in conversion of
 21 the carrier, i.e. $(1 - \bar{X}_{OC,in})$:

$$1 \quad t_{r,i} = \tau_i \left(1 - \bar{X}_{OC,in}\right) \quad (68)$$

2 To integrate Eq. (66) it is necessary to know $X_{OC}(t)$, which can be obtained taking into
 3 account the mean conversion of the carrier at the reactor inlet and the variation of
 4 conversion after a time t :

$$5 \quad X_{OC}(t) = \bar{X}_{OC,in} + \left[1 - \left(1 - \frac{t}{\tau_m}\right)^3\right] \quad (69)$$

6 The mean conversion of the particles, $\bar{X}_{OC,out}$, can be obtained as

$$7 \quad \left(1 - \bar{X}_{OC,out}\right) = \int_0^{\tau_m} \left(1 - X_{OC}(t)\right) E(t) dt \quad (70)$$

8 The mean reacting time, τ_m , can be determined by an iterative process to obtain from Eqs.
 9 (69) and (70) the corresponding mean conversion at the reactor outlet, $\bar{X}_{OC,out}$, that fit the
 10 mean conversion obtained from the mass balance to the whole reactor given by Eq. (54).
 11 Thus, a distribution of conversions is obtained.

12 The reaction rate of a particle with a conversion X_{OC} was calculated by using the gas
 13 concentration inside the particle, which was assumed to be constant over the entire particle,
 14 and equal to the gas concentration at the particle surface, $C_p = C_{ps}$. The gas concentration in
 15 the particle surface, C_{ps} , can be obtained by a mass balance to the whole particle taking into
 16 account the external diffusion through the gas film around the particle:

$$17 \quad \left(-\bar{r}_{g,i}\right)_{OC} = \frac{\rho_s R_{OC}}{b_i M_o} \left(\frac{4}{3} \pi r_p^3\right) \left[\frac{d\left(X_{OC}(t) - \bar{X}_{OC,in}\right)}{dt}\right]_i = k_{g,i} \left(4 \pi r_p^2\right) \left(C_{z,i} - C_{ps,i}\right) \quad (71)$$

18 The mass transfer coefficient for each gas, $k_{g,i}$, is obtained with equations proposed by
 19 Palchonok (1998) and Chakraborty and Howard (1981) for the bottom bed and the
 20 freeboard, respectively.

1 Bottom bed:
$$\text{Sh} = \frac{k_{g,i} d_p}{D_{g,i}} = 2\varepsilon_{mf} + 0.117\text{Ar}^{0.39}\text{Sc}^{1/3} \quad (72)$$

2 Freeboard:
$$\text{Sh} = \frac{k_{g,i} d_p}{D_{g,i}} = 2\varepsilon_z + 0.69\text{Re}_p^{1/2}\text{Sc}^{1/3} \quad (73)$$

3

4 2.3.2. Coal

5 In a previous work it was shown the relevance of the coal rank on the performance of the
 6 CLCC process (Cuadrat et al., 2012b). The carbon capture efficiency increased with
 7 increasing the char gasification rate or the volatile content in the coal. Besides, the oxygen
 8 demand decreased when the volatile content decreased. For simulations in this work, the
 9 bituminous “El Cerrejon” coal (Colombia), which is frequently used in power stations as
 10 fuel, is chosen. Its reactivity is between those of lignite and anthracite. The average particle
 11 size is assumed to be 125 μm , and the apparent density of char particles is 1100 kg/m^3 .

12 Table 5 shows the proximate and ultimate analysis of this coal.

13 When coal is fed to the fuel reactor different physical and chemical processes happen. First
 14 comes the drying and pyrolysis, where the moisture content and the volatile matter are
 15 evolved to the gaseous stream, as showed Eq. (37). Second, the remaining solid fraction,
 16 i.e. char which is mainly composed by carbon and mineral matter (ashes), is gasified.

17 The drying and pyrolysis processes are assumed to happen instantaneously in the feeding
 18 point of the coal. Pillai (1981) showed that the devolatilization times for several coals were
 19 lower than 2 s for particle size in the order of 0.5 mm at 1010 $^\circ\text{C}$. It is expected that the
 20 devolatilization time for smaller particles was lower, and it is believed that this time was
 21 lower than the mixing time of solids in the fuel reactor.

1 The product distribution during pyrolysis is calculated following the model described by
2 Matthesius et al. (1987). This model assumes the formation of carbon, CH₄, C₂H₆, tar, CO,
3 CO₂, H₂, H₂O, NH₃ and H₂S, which are calculated from the proximate and ultimate analysis
4 of the coal. At existing conditions in CLCC, it was found that no higher hydrocarbons than
5 CH₄ and very small amounts of tar were present in the gases (Cuadrat et al., 2011). Thus, it
6 is assumed that all C₂H₆ and tar predicted in the volatile matter were reformed by the
7 fluidizing gas, i.e. H₂O or CO₂, as it was previously done by Cuadrat et al. (2012c). With
8 these considerations, Table 7 shows the products distribution after drying and
9 devolatilization when H₂O was used as fluidization gas in the fuel reactor. The negative
10 values for H₂O were because some H₂O was taken from the fluidization gas flow for the
11 reforming of C₂H₆ and tar. H₂, CO and CH₄ present in the gaseous compounds are oxidized
12 by reaction with the oxygen carrier –see Eqs. (40-42)–. NH₃ was assumed to be
13 instantaneously converted into N₂, as this was the uniquely N-compound from the fuel
14 reactor (Song et al., 2012). Besides, SO₂ and COS was observed to be in much higher
15 concentration than H₂S in the fuel reactor, being SO₂ the major component (Shen et al.,
16 2010), indicating that sulphur compounds are not at thermodynamic equilibrium. Without
17 knowing the kinetics of oxidation of sulphur compounds by the oxygen carrier, it was
18 assumed that SO₂ was the only sulphur compound as an initial approach.
19 The carbon in the char is gasified with H₂O and CO₂, Eqs. (38-39). Assuming that
20 gasification proceeds according to the homogeneous model, the rates for the gasification
21 with H₂O or CO₂ are calculated as:

$$22 \quad \frac{1}{m_C} \left[\frac{dm_C}{dt} \right]_{H_2O} = \frac{1}{1 - X_C} \left[\frac{dX_C}{dt} \right]_{H_2O} = \frac{k_{H_2O} P_{H_2O}}{1 + K_{H_2O} P_{H_2O} + K_{H_2} P_{H_2}} \quad (74)$$

$$1 \quad \frac{1}{m_c} \left[\frac{dm_c}{dt} \right]_{\text{CO}_2} = \frac{1}{1 - X_c} \left[\frac{dX_c}{dt} \right]_{\text{CO}_2} = \frac{k_{\text{CO}_2} P_{\text{CO}_2}}{1 + K_{\text{CO}_2} P_{\text{CO}_2} + K_{\text{CO}} P_{\text{CO}}} \quad (75)$$

2 The gasification proceeds by the adsorption of the reacting gas in an active site in the char
3 surface, with an inhibitory effect of the products of reaction, i.e. H₂ for steam gasification
4 and CO for gasification with CO₂. Thus, the gasification rate decreases with increasing the
5 partial pressure of the product gas (H₂ or CO) because of an inhibitory effect. Kinetic
6 parameters were obtained in a previous work (Cuadrat et al., 2012c), and they are showed
7 in Table 6. The dependence on the temperature of the kinetic and adsorption constants, k_i
8 and K_i , was assumed to be Arrhenius type, similarly to Eq. (64) for kinetic constant for the
9 oxygen carrier reduction.

10 The net consumption or generation of the gas i by the char gasification, $(-\bar{r}_{g,i})_{char}$ to be used
11 in the mass balances -Eqs. (44) and (47)-, is given by

$$12 \quad (-\bar{r}_{g,i})_{char} = \frac{f_c \rho_s (1 - \varepsilon_z)}{M_c} \left[\frac{1}{m_c} \frac{dm_c}{dt} \right]_i \quad (76)$$

13 f_c being the mass fraction of carbon in the bed at a determined height. It was assumed that
14 the bed is composed by oxygen carrier and char particles. It is considered that ash particles
15 are not re-circulated from the air reactor, and only those in unconverted char are present.

16 This behaviour for ash particles was found by Cuadrat et al. (2011) in a 500 W_{th} CLCC
17 unit.

18 The carbon concentration in the fuel reactor, f_c , can be calculated in every phase j (bottom
19 bed, splash region or transport region) at every position z in the reactor from the
20 concentration of char and the char conversion as

$$21 \quad f_c = \left[\frac{C_{j,char}}{C_{j,char} + C_{j,OC}} \right] \left[\frac{(1 - X_{char}) [C]_{fix}}{(1 - X_{char}) [C]_{fix} + [ash]} \right] \quad (77)$$

1

2 2.4. Outputs from the model

3 The main outputs of the model are (1) the fluid dynamics structure of the reactor, e.g.
4 height of the bottom bed and profiles of concentration and flow of solids in the freeboard;
5 (2) the axial profiles of gas composition and flows (CO, H₂, CH₄, CO₂ and H₂O); (3) the
6 axial profile of char concentration in the reactor; (4) the axial profiles of average
7 conversions for the oxygen carrier and char; (5) the gas composition and solids flow in the
8 upper reactor exit to cyclone; and (6) the char flow to the air reactor. From these outputs the
9 performance of the CLCC system was assessed by analyzing the following parameters:

10 a) Oxygen demand of the flue gases. It represents the extent that coal is burned to CO₂ and
11 H₂O in the CLCC system. The total oxygen demand, Ω_T , is the fraction of oxygen
12 required to fully oxidize the unconverted gases exiting the fuel reactor to CO₂ and H₂O
13 with respect the total oxygen demand of the fuel, i.e. the stoichiometric amount of
14 oxygen required in an oxy-fuel process.

$$15 \quad \Omega_T = \frac{(F_{H_2} + F_{CO} + 4F_{CH_4})_{out}}{\Omega_{coal}} \quad (78)$$

16

17 To calculate the oxygen demand it is assumed that all char passing to the air reactor is
18 fully burned by air. Thus, unconverted products only come from the fuel reactor and the
19 oxygen demand depends on the combustion efficiency of gases generated in the fuel
20 reactor, i.e. both volatiles and gasification products. To better evaluate the oxygen
21 demand in the CLCC system, the combustion efficiency in the fuel reactor is defined as
22 the stoichiometric ratio of the oxygen transferred to the fuel in the fuel reactor versus the
oxygen demand of the coal converted in the fuel reactor:

$$\eta_{c,FR} = \frac{(F_{H_2O} + 2F_{CO_2} + F_{CO})_{out} - (F_{H_2O} + 2F_{CO_2} + F_{CO})_{in}}{\Omega_{coal} - 2F_{CO_2,AR}} \quad (79)$$

The oxygen transferred to the fuel, numerator in Eq. (79), is the oxygen supplied by the oxygen carrier, and it is calculated from an oxygen balance to gaseous compounds entering to and exiting from the reactor. The oxygen demanded by gaseous compounds evolved in the fuel reactor, denominator in Eq. (79), is calculated as the oxygen demanded by coal to be fully oxidized, Ω_{coal} , minus the oxygen demanded by carbon not emitted in the fuel reactor, i.e. $F_{CO_2,AR}$.

b) CO₂ capture efficiency. This parameter considers the physical removal of CO₂ that would otherwise be emitted into the atmosphere. It is defined as the fraction of the carbon introduced with coal that is converted to gas in the fuel reactor.

$$\eta_{CC} = M_C \frac{(F_{CO_2} + F_{CO} + F_{CH_4})_{out} - (F_{CO_2})_{in}}{[C]_{coal} \cdot F_{coal}} \quad (80)$$

Note that in this technology, the char that has not been gasified in the fuel reactor passes to the air reactor, it is burnt there to CO₂, and therefore it is not captured. The carbon capture efficiency depends on the char conversion, which was calculated in Eq. (59).

2.5. Calculation procedure

To solve the mathematical model developed with the above equations, convergence of the mass balance for solids and gases must occur simultaneously. For its solution, the model is solved using a Visual Fortran© code. The flow diagram for the overall solution of the model is shown in Fig. 3. To obtain the variation of the gases concentration with the height, the entire reactor is divided into compartments with a height of Δz .

- 1 The algorithm for the reactor model has the following calculation flow structure:
- 2 ○ Input data: the input data are the operating conditions and the characteristics of the
- 3 reactor, oxygen carrier and coal, as it is shown in Tables 1-7.
- 4 ○ Firstly, it is necessary to assign an initial value for the following parameters: (1)
- 5 dept of the bottom bed, $H_{b,0} = H_r/2$ is assumed as first estimation; (2) average
- 6 variation of the solids conversion in the reactor, which is estimated assuming full
- 7 combustion and carbon capture in the CLCC system, i.e.
- 8 $\Delta X_{OC,0} = M_O \Omega_{coal} F_{coal} / F_{OC} R_{OC}$; and (3) the carbon concentration in the bottom bed
- 9 is calculated as $f_{C,0} = \frac{0.5[C]_{fix} \cdot F_{coal}}{F_{OC}}$. The char concentration in the bottom bed is
- 10 calculated by using Eq. (77) assuming initially $X_{char} = 0.5$.
- 11 ○ The distribution of conversion for the oxygen carrier in the reactor is calculated
- 12 from Eqs. (69) and (70) to obtain $\Delta X_{OC} = \bar{X}_{OC,out} - \bar{X}_{OC,in}$.
- 13 ○ Fuel conversion: the mass balance for each reacting gas (CH_4 , CO , H_2 , CO_2 and
- 14 H_2O) is calculated in every compartment for the emulsion and bubble phases in the
- 15 bottom bed and the freeboard, see Eqs. (44), (45) and (47). The fluid dynamical
- 16 characteristics of the reactor (solids concentration and gas flow) are calculated
- 17 simultaneously to the mass balance. The system of differential equations for the
- 18 mass balance in every compartment is solved using a finite element method over the
- 19 entire reactor and starting from the distributor plate. A Runge–Kutta method is used
- 20 to solve the differential equations in every element of the reactor.
- 21 ○ Output data: when the mass balance for all the species is solved, the concentration
- 22 profiles of the gas species are obtained along the entire reactor, as well as the

1 variation with the height of fluid dynamical properties, e.g. gas flow distribution
2 and solids concentration. Eventually, the gas concentration of gases and solids
3 conversion at the reactor exit are determined. From these results, the variation of the
4 solids conversion, $\Delta X_{OC,1}$, is obtained from Eq. (54). Also the carbon gasified in the
5 whole reactor is calculated from Eq. (60).

6 ○ Convergence of pressure drop: from the profile of solids concentration, the pressure
7 drop in the fuel reactor is calculated, ΔP_1 . If $\Delta P_1 \neq \Delta P_0$, a new value of H_b is
8 considered.

9 ○ Convergence of oxygen balance: the variation of the solids conversion, $\Delta X_{OC,1}$,
10 obtained is compared to the assumed value. If $\Delta X_{OC,1} \neq \Delta X_{OC,0}$, the mass balance is
11 repeated using a new $\Delta X_{OC,0}$ value until reaching convergence.

12 ○ Convergence of carbon balance: from the carbon gasified in the whole reactor, the
13 carbon transferred to the air reactor is obtained from Eq. (56), $F_{C,AR,1}$. This value is
14 compared to the assumed $F_{C,AR,0}$ calculated from the assumed carbon concentration,
15 $f_{C,0}$, see Eqs. (57) and (58). If both values are not equal, a new value for $f_{C,0}$ is
16 assumed.

17 ○ Once the pressure balance and the mass balances for oxygen and carbon have
18 converged, the final results are obtained.

20 **3. Model results**

21 The developed model has been used to simulate the behaviour of the fuel reactor in the 1
22 MW_{th} CLCC plant erected in TU Darmstadt (Ströhle et al., 2010). Preliminary predictions
23 from the model has been obtained by using a value for the efficiency of the carbon

1 separation system of 0.9. Besides, the water-gas shift (WGS) reaction, see Eq. (43), was not
2 considered in the calculations as a first approximation because in previous works it was
3 found that this reaction had low relevance in the coal conversion using ilmenite as oxygen
4 carrier (Cuadrat et al., 2012d and 2012e). Later, simulations were done to analyze the effect
5 of the carbon separation system efficiency, from 0 to 1, on the CLCC process performance.

6

7 *3.1. Analysis of the fuel reactor performance*

8 The reference case has been simulated, i.e. the design conditions showed in Table 1 and
9 reference conditions in Table 2 were used. Note that the efficiency of the carbon separation
10 system was fixed to be $\eta_{\text{CSS}} = 0.9$. The performance of the CLCC is made by analyzing two
11 parameters: the carbon capture and the oxygen demand. Two additional parameters, i.e. the
12 char conversion and the combustion efficiency in the fuel reactor are also used here to
13 better understand the performance of the fuel reactor. From now on, these four parameters
14 will be appointed as the “evaluating parameters”. In the reference case analyzed in this
15 section, the carbon capture efficiency predicted was $\eta_{\text{CC}} = 59\%$. This low value is due to
16 the low char conversion reached in the fuel reactor, $X_{\text{char}} = 42\%$. The oxygen demand was
17 $\Omega_{\text{T}} = 10.5\%$, coming from unconverted volatile matter and also from product of char
18 gasification in the freeboard. The predicted combustion efficiency in the fuel reactor was
19 $\eta_{\text{c,FR}} = 83.7\%$.

20 To evaluate these global results of the CLCC performance, a deeper analysis is done where
21 the gas and solids profiles, and the distribution of reaction rates are presented. Figs. 4(a)
22 and (b) shows the axial profiles of gases and solids flow, and Figs. 4(c) and (d) shows the

1 axial profiles of gas and solids concentration in the fuel reactor. Also the gas velocity is
2 plotted in Fig. 4(b).

3 The gas flow increases through the reactor because gases generated during coal
4 gasification. Also, abrupt changes in gas flow are found at the positions where the coal is
5 fed ($z = 0.1$ m) and the char separated in the carbon stripper is recirculated ($z = 0.2$ m), see
6 Fig. 4(a). This was because the evolution of volatile matter in the first case, and the gas
7 coming from the carbon stripper in the second case. Note that the flow from the carbon
8 stripper is almost three times the gas flow introduced by the distributor plate. Although the
9 gas flow is increasing throughout the entire reactor, a decrease in the gas velocity is
10 observed in the upper part of the reactor ($z > 9$ m). This fact was because the core section
11 only increases above the height which the saturation value in the annulus is reached, see
12 Eqs. (17-19). As gas was assumed to flow by the core, the gas velocity decreases as the
13 core section increases above $z_{\text{sat}} = 9$ m.

14 From the profiles of solids concentration, the separation of the bottom bed and the
15 freeboard can be easily observed. The bottom bed is stretched out to a height of $H_b = 0.58$
16 m, being characterized by a roughly constant porosity. Above the bottom bed, the solids
17 concentration decreases with the reactor height. Until a height of 3 m the solids
18 concentration is dominated by the splash phase. The solids concentration in the splash
19 phase falls out to values close to 0 at higher heights. In the upper half-reactor, the transport
20 phase prevails and the solids concentration is low. In addition, the solids in the transport
21 phase are enriched in char as they go up through the riser (see Fig. 4), because of the lower
22 terminal velocity of char particles. Regarding the solids flow, which is represented in Fig.
23 4(b), there is a net solids flow upward through the core region in the transport phase. The
24 flow of solids decreases with the axial position as a part of solids are being transferred from

1 the core to the annulus region. Besides, a change in the solids flow tendency is appreciated
2 at a height of $z = 9$ m. This fact is linked to the decrease in the gas velocity above this
3 position. In particular, the decay constant for the solids concentration in transport phase, K_i ,
4 increases as the gas velocity decreases, see Eq. (23). As consequence, both concentration
5 and flow of solids in the transport phase decrease quicker when the gas velocity decreases
6 with the reactor height.

7 To better appreciate the behaviour of the fuel reactor in the bottom bed, the profiles of
8 gases in the emulsion, the bubbles and the average in the bottom bed are showed in detail in
9 Figs. 5(a)-(c). At the bottom of the bed, the gas is mainly composed by H_2O , which is the
10 fluidization gas. The carbon gasification and reaction of gases with the oxygen carrier
11 proceed in the emulsion phase. So, downstream the gas is gaining on CO_2 , which is
12 concentrated in the emulsion phase. This means that the carbon mixed with the oxygen
13 carrier is being gasified. The product gases (CO and H_2) are evolved to the emulsion phase
14 and they are quickly oxidized to CO_2 and H_2O by the oxygen carrier. Moreover, the rate of
15 CO_2 generation is faster than the rate of gas diffusion from the emulsion to the bubbles,
16 indicated by the build up of CO_2 in the emulsion phase.

17 It can be seen a strong change on gas concentration and gas velocity at $z = 0.1$ and $z = 0.2$
18 m, that is at the coal and recirculated char feeding points, respectively. At the feeding point
19 of coal, the volatile matter is evolved to the gas phase, increasing the concentration of CH_4 ,
20 CO , H_2 , and CO_2 , i.e. the main components in the volatile matter (see Table 7). Volatile
21 matter reacts slower than the products from carbon gasification, because the volatile matter
22 is evolved to the bubble phase, and it must diffuse to the emulsion phase to react with the
23 oxygen carrier. At the height where the recirculated char from the carbon stripper is
24 introduced, it is observed an increase of the H_2O content, and consequently the other gases

1 are diluted. This H₂O proceeds from the gas used to fluidize the carbon stripper (steam).
2 After the feeding point of the recirculated char, the gases in emulsion are being enriched in
3 steam by diffusion from the bubbles, which has a higher concentration and flow of steam.
4 This proceeds until steam concentration is similar both in emulsion and bubble phase. Both
5 gasification products generated in the emulsion and volatile matter diffusing from the
6 bubbles react in the emulsion with the oxygen carrier particles. Nevertheless, CO₂ mainly
7 proceeds from conversion of CO from carbon gasification rather than reaction of volatile
8 matter evolved to the bubble phase, because the slow diffusion of gases among the bubble
9 and the emulsion phases. Thus, CO₂ concentration slightly increases in the emulsion,
10 whereas volatile matter slowly decreased its concentration in bubbles. A counter-current
11 diffusion of CO₂ and H₂O from emulsion to bubbles also happens in this section.
12 Eventually, in the emulsion phase the concentration of gases level out, because it is reached
13 a pseudo–equilibrium where the rates of generation of CO₂ and H₂O in the emulsion phase
14 are balanced by the amount of these gases disappearing by char gasification and diffusing
15 to the bubble phase.
16 When the top of the bottom bed is reached, the gas in the emulsion and bubble is mixed,
17 which is observed when Fig. 4(c) and Figs. 5(a-c) are compared. Because the flow through
18 the bubbles is much higher than the flow through the emulsion, the gas composition in the
19 freeboard is dominated by the gaseous components in the bubbles. Thus, the concentration
20 of H₂, CO, and CH₄ seen by the oxygen carrier is increased, increasing the reaction rate of
21 the oxygen carrier. As a consequence, the H₂, CO and CH₄ concentrations decrease rapidly
22 while the splash phase is prevailing in the freeboard. Volatile matter, which was hardly
23 converted in the bottom bed, was mainly oxidized in the splash phase. Where the transport

1 phase prevails over the splash phase ($z > 3$ m) the gas flow and composition barely changes
2 because of the low amount of reacting solids.
3 Additional information about the conversion of gases in the bottom bed and freeboard can
4 be drawn from the analysis of the oxygen demand of gases as a function of the reactor
5 height, see Fig. 6(a). The oxygen demand slowly decreases in the bottom bed due to the
6 slow conversion of volatile matter, which mainly flows through the bubbles. Likewise, the
7 oxygen demand decreases in the freeboard until a height about 3 m, mainly due to the
8 conversion of volatile matter. Later, the oxygen demand is roughly constant because of the
9 low solids concentration and a pseudo-equilibrium is reached between CO and H₂
10 generation by gasification and consumption by reaction with the oxygen carrier.

11 An analysis of the volumetric rate of gasification, $(-r'_C)$, and oxygen transference $(-r'_O)$
12 can explain the gas concentration profiles in the bottom bed and freeboard, besides the
13 oxygen demand evolution. These reaction rates were calculated as:

14 In the bottom bed:

$$15 \quad (-r'_C) = (1 - \delta_b) \left[(-\bar{r}_{g,H_2O})_{char} + (-\bar{r}_{g,CO_2})_{char} \right]_e \quad (81)$$

$$16 \quad (-r'_O) = (1 - \delta_b) \left[(-\bar{r}_{g,H_2})_{OC} + (-\bar{r}_{g,CO})_{OC} + 4(-\bar{r}_{g,CH_4})_{OC} \right]_e \quad (82)$$

17 In the freeboard:

$$18 \quad (-r'_C) = \left[(-\bar{r}_{g,H_2O})_{char} + (-\bar{r}_{g,CO_2})_{char} \right]_{spl} - \left[(-\bar{r}_{g,H_2O})_{char} + (-\bar{r}_{g,CO_2})_{char} \right]_{tr} \quad (83)$$

$$19 \quad (-r'_O) = \xi_{g-s} \left[(-\bar{r}_{g,H_2})_{OC} + (-\bar{r}_{g,CO})_{OC} + 4(-\bar{r}_{g,CH_4})_{OC} \right]_{spl} \quad (84)$$

$$+ \xi_{g-s} \left[(-\bar{r}_{g,H_2})_{OC} + (-\bar{r}_{g,CO})_{OC} + 4(-\bar{r}_{g,CH_4})_{OC} \right]_{tr}$$

1 Fig. 6(b) shows the axial profiles of both reaction rates, as well as the ratio $(-r'_o)/(-r'_c)$.
2 The oxygen transference rate and the gasification rate are roughly constant in the bottom
3 bed because solids were assumed to be homogeneously distributed. At $z < 0.1$ m the ratio
4 $(-r'_o)/(-r'_c)$ was about 2, indicating that the entire carbon gasified is oxidized to CO₂ (one
5 atom of carbon needs two atoms of oxygen). Above coal feeding point the ratio
6 $(-r'_o)/(-r'_c)$ was about 3, which indicates that some oxygen transferred is used to oxidize
7 volatile matter diffusing from bubbles; nevertheless, most of oxygen is used to oxidize
8 gasification products generated in the emulsion.
9 When the gas passes from the bottom bed to the freeboard, the rate of oxygen transference
10 increases and the rate of gasification decreases. Although the contact efficiency, ξ_{g-s} , in the
11 region just above the bottom bed is low, the higher concentration of reducing gases in the
12 freeboard regarding the bottom bed the higher oxygen transference rate. Nevertheless, the
13 oxygen transference rate rapidly decreases as the solids concentration in the freeboard falls.
14 The gasification rate decreases when gases enters into the freeboard, because char particles
15 are seeing a higher concentration of H₂ and CO, which inhibits the carbon gasification.
16 The ratio $(-r'_o)/(-r'_c)$ reaches high values at the beginning of the freeboard, and it
17 decreases as the solids and reducing gas (H₂, CO and CH₄) concentration decreases. This
18 fact indicates the relevance in the splash phase of volatile matter oxidation. Above the
19 splash phase, a new pseudo-equilibrium is reached where the ratio $(-r'_o)/(-r'_c)$ approaches
20 to a value of 2, indicating that the CO and H₂ generated by gasification is balanced by its
21 oxidation to CO₂ and H₂O. Nevertheless, as the upper part of the freeboard the solids

1 concentration is low and the gas flow rate is high, the gas concentration barely is affected
2 by the gas–solid reactions.

3 It is relevant to clarify the differences between the use of a gaseous fuel and a solid fuel.
4 Abad et al. (2010) modelled the combustion of CH₄ with a Cu-based oxygen carrier in a 10
5 kW_{th} CLC unit. They showed that the conversion rate of methane was particularly reduced
6 in the two-third upper part of the bottom bed. In this zone, most of unconverted gas is going
7 through the bubble phase, and the gas conversion was mainly limited by the gas transfer
8 between bubble and emulsion. Instead, when a solid fuel is used, an important amount of
9 oxygen transferred is used to convert the products from carbon gasification in the bottom
10 bed. Moreover, in the bottom bed the carbon gasification is enhanced by the reaction of H₂
11 and CO with the oxygen carrier to produce the gasification agents (H₂O and CO₂). In fact,
12 the gasification rate was highest in the bottom bed. Similar to the case for gaseous fuels, the
13 conversion of volatile matter is low in the bottom bed.

14 In the freeboard, the concentration of reducing gases is low when solid fuels are used,
15 because dilution with a high flow of fluidization gas, i.e. H₂O in this case. However, the
16 fuel conversion is faster for gaseous fuels, because the oxygen carrier reacts with a gas
17 highly concentrated in the fuel gas. As consequence, the relative increase in the rate of
18 oxygen transference when gas passes to freeboard with solid fuels is lower than with
19 gaseous fuels. In addition, CO and H₂ are being continuously generated by carbon
20 gasification, which do not react with the oxygen carrier as quick as in the bottom bed. This
21 fact causes the accumulation of CO and H₂ in the gas, preventing the complete conversion
22 of gases to CO₂ and H₂O. Of the above, the conversion of the gases towards CO₂ and H₂O
23 would be lower with solid fuels than with gaseous fuels.

24

1 *3.2. Efficiency of carbon separation in the carbon separation system*

2 An external carbon separation system, e.g. a carbon stripper, has been proposed as the
3 better solution to increase the carbon capture in the CLCC process (Kramp et al., 2012). In
4 the reference case analyzed in this work with a carbon separation efficiency $\eta_{CCS} = 90\%$ it
5 was obtained a carbon capture of $\eta_{CC} = 59\%$. It seems that a higher value of the carbon
6 separation efficiency should be necessary to increase the carbon capture of the CLCC
7 system. Indeed, the efficiency of the carbon separation system has been identified a key
8 factor in order to reach high carbon capture in a CLCC system (Cuadrat et al., 2012c;
9 Kramp et al., 2012; Ströhle et al., 2009). Thus, an analysis of the carbon separation system
10 efficiency on the CLCC system behaviour is done in this section.

11 Figs. 7(a) shows the evaluating parameters for the design and operating conditions showed
12 in Tables 1 and 2. The carbon separation efficiency was varied from 0 to 1. It can be seen
13 that all the evaluating parameters increase as the carbon separation efficiency increases. As
14 the carbon separation efficiency increases, the loss of carbon towards the air reactor
15 decreases. Consequently, the carbon evolved to the gas phase in the fuel reactor increases,
16 i.e. the carbon capture increases. The real effect of the carbon separation system is to
17 modify the residence time of char particles into the fuel reactor by varying the char
18 concentration mixed together ilmenite particles, see Fig. 7(b). Thus, an increase of the
19 efficiency of carbon separation causes an increase of the char concentration in the bed, and
20 therefore, an increase of the char flow to the cyclones and the carbon stripper, which should
21 be taken into account for the performance of the carbon separation system. Also, the flow
22 of solids that must be managed by cyclones and/or carbon stripper increases as the
23 efficiency of the carbon separation system increases because a higher flow of solids

1 internally circulating between the fuel reactor and the cyclone-carbon stripper system. In
2 addition, the gas generated in the fuel reactor increases, and a higher flow of solids is
3 entrained to the cyclone.
4 On the contrary, the oxygen demand from the flue gases increases because the flow of
5 reacting gases increases, whereas the ilmenite hold-up is maintained constant. This fact is
6 due to the high generation of CO in a freeboard highly concentrated in char particles. Thus,
7 the combustion efficiency in the fuel reactor was decreased as the char concentration in the
8 bed was increased, i.e. the carbon separation system was more efficient. Indeed, when the
9 efficiency of carbon separation was 1, the combustion efficiency would be about 75%,
10 whereas the oxygen demand was 25%. Note that in this case as $F_{CO_2,AR} = 0$, it is fulfilled
11 that $\Omega_T = 1 - \eta_{c,FR}$, see Eqs. (78) and (79). At this condition, the char concentration in the
12 bottom bed was 3 wt.%, reaching 10 wt.% at the top of the fuel reactor, and the CO
13 concentration at the exit increases up to 12.5 vol.%.

14

15 **4. Discussion**

16 From the results showed in this work, the performance of the CLCC system at the base case
17 produced low carbon capture values ($\eta_{CC} = 59\%$) and relatively high oxygen demand ($\Omega_T =$
18 10.5%). An increase of the carbon separation system efficiency increases the carbon
19 capture, but also increases the oxygen demand. The solids hold-up in the 1 MW_{th} high-
20 velocity fluidized-bed reactor was 260 kg, and the mean residence time of oxygen carrier
21 particles was 100 s. The values of carbon capture were similar to that predicted by a model
22 of a bubbling fluidized bed, but the oxygen demand was lower (Cuadrat et al., 2012c). This
23 fact shows the better performance of a high-velocity fluidized bed burning the gases

1 generated in the reactor compared to that of a bubbling fluidized bed. The residence time
2 was much lower than the assumed by Kramp et al. (2010), and lower than the required to
3 reach high carbon capture (Cuadrat et al., 2012c; Ströhle et al., 2009).

4 The formulated macroscopic model consisted in semi-empirical equations which have
5 intrinsically some uncertainties. Therefore, it would be very interesting to validate the
6 model against experimental results available in the future, both for the fluid dynamics and
7 the coal conversion process.

8 In addition, the CLCC system should be optimized in order to improve the carbon capture
9 and to decrease the oxygen demand, e.g. increasing the temperature, the solids hold-up, or
10 using a more reactive oxygen carrier. These issues will be addressed in the next work by
11 using the developed model.

12

13 **5. Conclusions**

14 A model to describe the behaviour of the fuel reactor of a Chemical–Looping Coal
15 Combustion (CLCC) process has been developed. The model considers the processes
16 affecting the reaction of fuel with the oxygen carrier, such as reactor fluid dynamics,
17 reactivity of the oxygen carrier and the gasification reactivity. The fuel reactor simulation is
18 based on the erected 1 MW_{th} CLCC unit at TU Darmstadt, which is considered to be a
19 fluidized bed at the high velocity regime. Also the effect of a carbon separation system on
20 the fuel reactor performance is evaluated.

21 Predictions of the model showed that conversion of char particles is enhanced in the bottom
22 bed. In this region, the concentration of gasification products, i.e. H₂ and CO, are
23 maintained at low values because they are continuously removed by reaction with the
24 oxygen carrier, reaching a pseudo-equilibrium state. In the freeboard, there is an

1 accumulation of the gasification products, and the splash phase was primarily the
2 responsible of volatile matter conversion. Solids in the upper part of the fuel reactor are
3 being concentrated in char particles, and extension of chemical reactions is low because of
4 the low concentration of solids.

5 The conversion of coal is limited by gasification in the bottom bed. At the reference case
6 analyzed in this work, the carbon capture efficiency is 59%, being rather a low value
7 because the low char conversion in the reactor. The oxygen demand is 10.5%, mainly due
8 to unburnt volatile matter.

9 The CLCC system should be optimized in order to improve the carbon capture and to
10 decrease the oxygen demand. A key issue to reach high carbon capture is to increase the
11 efficiency of carbon separation system. The carbon capture efficiency is 95% if the carbon
12 separation efficiency was increased to a value as high as 99%.

13

14

15

16 **Acknowledgment**

17 This work was partially supported by the European Commission, under the RFCS Program
18 (ECLAIR Project, Contract RFCP-CT-2008-0008), and from Alstom Power Boilers.

19

20

1 Nomenclature

2

3 a = decay factor for the solids concentration in the splash phase

4 A_0 = area of the gas-distributor per nozzle, m^2 per nozzle

5 A_c = cross section area of core, m^2

6 A_w = cross section area of the annulus, m^2

7 Ar = Archimedes number

8 b_i = stoichiometric coefficient for metal oxide in combustion of gas i

9 C_1 = constant in Eq. (2)

10 C_2 = constant in Eq. (2)

11 C_b = concentration of solids in the bottom bed, kg m^{-3}

12 $C_{b,i}$ = concentration of gas i in the bubble phase, mol m^{-3}

13 C_C = char concentration, kg of char per kg of solids

14 C_{dil} = concentration of solids in the freeboard, kg m^{-3}

15 $C_{dil,i}$ = concentration of gas i in the freeboard, mol m^{-3}

16 $C_{e,i}$ = concentration of gas i in the emulsion phase, mol m^{-3}

17 $C_{p,i}$ = concentration of gas i in the particle, mol m^{-3}

18 $C_{ps,i}$ = concentration of gas i at the particle's surface, mol m^{-3}

19 C_{spl} = concentration of solids in the splash phase, kg m^{-3}

20 C_{tr} = concentration of solids in the transport phase, kg m^{-3}

21 C_w = solids concentration in the annulus, kg/m^3

22 C_z = gas concentration in the bulk gas at the height z , mol/m^3

23 d_b = diameter of bubble, m

24 d_i = stoichiometric coefficient for O_2 in the combustion of gas i

- 1 d_p = average diameter of particles, m
- 2 d_{react} = inside diameter of the reactor, m
- 3 D_g = gas diffusivity, m^2/s
- 4 $E(t)$ = residence time distribution curve
- 5 $E_{a,i}$ = activation energy, kJ/mol
- 6 f_b = empirical function given by Eq. (7)
- 7 f_C = mass fraction of carbon in the bed (-)
- 8 $f_{C,fx}$ = fraction of fixed carbon in coal
- 9 F_0 = flow rate of solids entrained from the bottom bed, kg/s
- 10 $F_{b,i}$ = flow of gas i in the bubble phase, mol/s
- 11 F_c = solids flow by the core, kg/s
- 12 F_{coal} = rate of coal feeding, kg/s
- 13 $F_{C,AR}$ = flow of carbon to the air-reactor, mol/s
- 14 $F_{C,FR}$ = flow of carbon exiting from the fuel-reactor, mol/s
- 15 $F_{C,in}$ = flow of carbon in coal fed, mol/s
- 16 $F_{\text{dil},i}$ = flow of gas i in the dilute phase, mol/s
- 17 $F_{e,i}$ = flow of gas i in the emulsion phase, mol/s
- 18 F_{exc} = excess of flow in the emulsion over the minimum fluidization condition, mol/s
- 19 $F_{g,CS}$ = gas flow from the carbon stripper, Nm^3/s
- 20 $F_{g,in}$ = inlet gas flow, Nm^3/s
- 21 F_i = molar flow of gas i , mol/s
- 22 F_{OC} = solids circulation rate, kg/s
- 23 F_s = solid flow going to cyclone, kg/s

- 1 F_t = solid flow from the core to the annulus, kg/s
- 2 F_w = solids flow by the wall–layer, kg/s
- 3 $F_{WGS,i}$ = flow of gas i due to the WGS reaction, mol/s
- 4 g = acceleration due to gravity, $m^2 s^{-1}$
- 5 H_b = upper bottom bed height, m
- 6 H_{Coal} = height of the coal feeding, m
- 7 H_{CS} = height of the char feeding, m
- 8 H_r = height of the reactor, m
- 9 $k_{0,i}$ = preexponential factor of the kinetic constant, $mol^{1-n} m^{3n-2} s^{-1}$
- 10 k_b = backflow ratio
- 11 k_{bc} = mass transfer coefficient between bubble and emulsion, s^{-1}
- 12 k_g = external gas mass transfer coefficient, s^{-1}
- 13 k_i = kinetic constant, $mol^{1-n} m^{3n-2} s^{-1}$
- 14 K = decay factor for the solids concentration in the transport phase
- 15 n = reaction order
- 16 m_C = mass of carbon in char particles, kg
- 17 M_C = atomic mass of carbon, kg/mol
- 18 M_O = atomic mass of oxygen, kg/mol
- 19 N_{nz} = number of nozzles in the distributor plate
- 20 P = pressure at the reactor outlet, Pa
- 21 P_i = partial pressure of gas i , atm
- 22 r_g = grain radius, m
- 23 $(-\bar{r}_{g,i})_{OC}$ = average reaction rate of gas i with the oxygen–carrier, $mol m^{-3} s^{-1}$

- 1 $(-\bar{r}_{g,i})_{char}$ = average reaction rate of gas i with char, mol m⁻³ s⁻¹
- 2 $(-\bar{r}_{OC,i})$ = average reaction of oxygen in the oxygen-carrier, mol m⁻³ s⁻¹
- 3 r_p = particle radius, m
- 4 R_g = constant of ideal gases, J mol⁻¹ K⁻¹
- 5 R_{OC} = oxygen transport capacity of the oxygen-carrier
- 6 Re = Reynolds number
- 7 S_{react} = cross section area of the reactor, m²
- 8 Sc = Schmidt number
- 9 Sh = Sherwood number
- 10 t = time, s
- 11 t_{mr} = mean residence time of solids in the reactor, s
- 12 t_r = reacting time of solid from zero conversion until the maximum variation in solid
- 13 conversion, s
- 14 T = temperature of the fuel-reactor, K
- 15 $u_{b\infty}$ = velocity of a single bubble, m s⁻¹
- 16 $u_{s,c}$ = velocity of solids in the core, m s⁻¹
- 17 u_g = gas velocity in the reactor, m/s
- 18 u_{mf} = gas velocity at minimum fluidization condition, m/s
- 19 u_t = terminal velocity of particles, m/s
- 20 u_{tf} = throughflow of gas in the bottom bed, m/s
- 21 u_{vis} = visible gas flow in the bubbles, m/s
- 22 $u_{vis,sat}$ = visible gas flow in the bubbles at saturation condition, m/s
- 23 V = volume, m³

- 1 x = stoichiometric factor for carbon in the hydrocarbon C_xH_y
- 2 X_C = conversion of carbon in char
- 3 X_{OC} = conversion of the oxygen-carrier
- 4 $\bar{X}_{OC,in}$ = average conversion of the oxygen-carrier at the fuel-reactor inlet
- 5 $\bar{X}_{OC,out}$ = average conversion of the oxygen-carrier at the fuel-reactor outlet
- 6 X_s = solids conversion
- 7 y = stoichiometric factor for hydrogen in the hydrocarbon C_xH_y
- 8 $y_{e,i}$ = molar fraction of gas i in the emulsion
- 9 z = height or vertical position in the reactor, m
- 10 z_{coal} = height of the feeding point of coal, m
- 11 z_{CS} = height of the feeding point of solids from the carbon stripper, m
- 12 z_{sat} = height at which the saturation value is reached, m
- 13
- 14 Greek symbols:
- 15 δ_b = volumetric fraction of bubbles in the bottom bed
- 16 $\delta_{b,sat}$ = fraction of bubbles in the bottom bed at saturation condition
- 17 δ_w = thickness of the annulus, m
- 18 $\delta_{w,sat}$ = thickness of the annulus at saturation conditions, m
- 19 ΔP_0 = pressure drop in the reactor, Pa
- 20 ΔX_{OC} = variation of the conversion of oxygen-carrier in the reactor
- 21 ε_b = bed porosity
- 22 $\varepsilon_{b,sat}$ = bed porosity at saturation condition
- 23 ε_z = porosity in the freeboard

- 1 ε_{mf} = porosity at minimum fluidization condition
- 2 ϕ_i = sphericity of particles i
- 3 ϕ_{oc} = ratio of oxygen-carrier to fuel
- 4 ϕ_{H_2O} = ratio of steam to coal, kg of steam per kg of coal
- 5 μ_g = viscosity of gas, $\text{kg m}^{-1} \text{s}^{-1}$
- 6 η_c = combustion efficiency
- 7 $\eta_{C, gas}$ = gasification efficiency
- 8 η_{CSS} = efficiency of the carbon separation system
- 9 ρ_g = gas density, kg/m^3
- 10 ρ_i = apparent density of solids i, kg/m^3
- 11 ρ_m = molar density, mol/m^3
- 12 ρ_s = average density of solids, kg/m^3
- 13 $\sum F_{O, in}$ = molar flow of oxygen atoms in the compounds entering to the fuel-reactor,
- 14 mol/s
- 15 $\sum F_{O, out}$ = molar flow of oxygen atoms in the compounds exiting from the fuel-reactor,
- 16 mol/s
- 17 ξ_{g-s} = efficiency of contact between gas and solids in the freeboard
- 18 τ_i = time for complete solid conversion, s
- 19 τ_m = time for complete conversion of solid at the average gas concentration in the reactor, s
- 20 Ω_{coal} = oxygen demand of coal, mol of oxygen per kg of coal
- 21 Ω_O = oxygen demand of gases
- 22 Ψ = ratio of the visible bubble flow to the total flow through the bubbles

- 1 Ψ_{sat} = ratio of the visible bubble flow to the total flow through the bubbles at saturation
- 2 condition
- 3

1 **References**

- 2
- 3 Abad, A., Adánez, J., García-Labiano, F., de Diego, L.F., Gayán, P., Celaya, J., 2007
- 4 Mapping of the range of operational conditions for Cu-, Fe-, and Ni-based oxygen
- 5 carriers in chemical-looping combustion. *Chemical Engineering Science* 62, 533-549.
- 6 Abad, A., Adánez, J., García-Labiano, F., de Diego, L.F., Gayán, P., 2010. Modeling of the
- 7 chemical-looping combustion of methane using a Cu-based oxygen-carrier. *Combustion*
- 8 and *Flame*, 157, 602-615.
- 9 Abad, A., Adánez, J., Cuadrat, A., García-Labiano, F., Gayán, P., de Diego, L.F., 2011.
- 10 Kinetics of redox reactions of ilmenite for chemical-looping combustion. *Chemical*
- 11 *Engineering Science* 66, 689–702.
- 12 Abdulally, I., Beal, C., Herbert, A., Epple, B., Lyngfelt, A., Bruce, L., 2012. Alstom’s
- 13 Chemical Looping Prototypes, Program Update. Proc. From the 37th Int. Technical Conf.
- 14 on Clean Coal & Fuel Systems, June 3-7, 2012, Clearwater, FL, USA.
- 15 Adánez, J., Gayán, P., de Diego, L.F., García-Labiano, F., Abad, A., 2003. Combustion of
- 16 Wood Chips in a CFBC. Modeling and Validation. *Industrial Engineering Chemistry*
- 17 *Research* 42, 987-999.
- 18 Adánez, J., Cuadrat, A., Abad, A., Gayán, P., de Diego, L.F., García-Labiano, F., 2010.
- 19 Ilmenite Activation during Consecutive Redox Cycles in Chemical-Looping
- 20 Combustion. *Energy Fuels* 24, 1402–1413.
- 21 Adánez, J., 2012. Chemical-looping combustion of coal: recent developments and
- 22 technology challenges. Proceedings from the 21st Int. Conf. on Fluidized Bed
- 23 Combustion, Naples (Italy), 4-6 June 2012.

- 1 Adanez, J., Abad, A., Garcia-Labiano, F., Gayan, P., de Diego, L.F., 2012. Progress in
2 Chemical-Looping Combustion and Reforming technologies. *Progress in Energy and*
3 *Combustion Science* 38. 215-282.
- 4 Berguerand, N., Lyngfelt, A., 2008a. Design and operation of a 10 kW_{th} chemical-looping
5 combustor for solid fuels – Testing with South African coal. *Fuel* 87, 2713–2726.
- 6 Berguerand, N., Lyngfelt, A., 2008b. The use of petroleum coke as fuel in a 10 kW_{th}
7 chemical-looping combustor. *Int. J. Greenhouse Gas Control* 2, 169–179.
- 8 Berguerand, N., Lyngfelt, A., 2009. Chemical-Looping Combustion of Petroleum Coke
9 Using Ilmenite in a 10 kW_{th} Unit-High-Temperature Operation. *Energy Fuels* 23, 5257–
10 5268.
- 11 Broadhurst, T.E., Becker, H.A., 1975. Onset of fluidization and slugging in beds of uniform
12 particles. *AIChE J.* 21, 238-247.
- 13 Brown, T.A., Dennis, J.S., Scott, S.A., Davidson, J.F., Hayhurst, A.N., 2010. Gasification
14 and Chemical-Looping Combustion of a Lignite Char in a Fluidized Bed of Iron Oxide.
15 *Energy Fuels* 24, 3034-3048.
- 16 Chakraborty, R.K., Howard, J.R., 1981. Combustion of char in shallow fluidized bed
17 combustors: influence of some design and operating parameters. *J. Inst. Energy*, 1981,
18 54, 48-54.
- 19 Cuadrat, A., Abad, A., García-Labiano, F., Gayán, P., de Diego, L.F., Adánez, J., 2011. The
20 use of ilmenite as oxygen-carrier in a 500 W_{th} Chemical-Looping Coal Combustion unit.
21 *Int. J. Greenhouse Gas Control* 5, 1630–1642.
- 22 Cuadrat, A., Abad, A., García-Labiano, F., Gayán, P., de Diego, L.F., Adánez, J., 2012a.
23 Effect of operating conditions in Chemical-Looping Combustion of coal in a 500 W_{th}
24 unit. *Int. J. Greenhouse Gas Control* 6, 153–163.

- 1 Cuadrat, A., Abad, A., García-Labiano, F., Gayán, P., de Diego, L.F., Adánez, J., 2012b.
2 Relevance of the coal rank on the performance of the in situ gasification chemical-
3 looping combustion. *Chemical Engineering Journal* 195-196, 91–102.
- 4 Cuadrat, A., Abad, A., Gayán, P., de Diego, L.F., García-Labiano, F., Adánez, J., 2012c.
5 Theoretical approach on the CLC performance with solid fuels: Optimizing the solids
6 inventory. *Fuel* 97, 536-551.
- 7 Cuadrat, A., Abad, A., Adánez, J., de Diego, L.F., García-Labiano, F., Gayán, P., 2012d.
8 Behavior of ilmenite as oxygen carrier in chemical-looping combustion. *Fuel Processing*
9 *Technology* 94, 101-112.
- 10 Cuadrat, A., Abad, A., de Diego, L.F., García-Labiano, F., Gayán, P., Adánez, J., 2012e.
11 Prompt considerations on the design of Chemical-Looping Combustion of coal from
12 experimental tests. *Fuel* 97, 219-232.
- 13 Darton, R.C., LaNauze, R.D., Davidson J.F., Harrison, D., 1977. Bubble growth due to
14 coalescence in fluidized beds. *Trans IChemE* 55.
- 15 de Diego, L.F., Gayán, P., Adánez, J., 1995. Modelling of flow structure in circulating
16 fluidized beds. *Powder Technology* 85, 19-27.
- 17 Dewaele, O., Froment, G.F., 1999. TAP Study of the Mechanism and Kinetics of the
18 Adsorption and Combustion of Methane on Ni/Al₂O₃ and NiO/Al₂O₃. *Journal of*
19 *Catalysis* 184, 499-513.
- 20 Foka, M., Chaouki, J., Guy C., Klvana, D., 1996. Gas phase hydrodynamics of a gas-solid
21 turbulent fluidized bed reactor. *Chemical Engineering Science* 51, 713-723.
- 22 Furusaki, S., Kikuchi, T., Miyauchi, T., 1976. Axial Distribution of Reactivity Inside a
23 Fluid-Bed Contactor. *AIChE J.* 22, 354-361.

- 1 Galloy, A., Ströhle, J., Epple, B., 2011. Design and operation of a 1 MWth carbonate and
2 chemical looping CCS test rig. VGB PowerTech 6.
- 3 García-Labiano, F., de Diego, L.F., Adánez, J., Abad, A., Gayán, P., 2004. Reduction and
4 Oxidation Kinetics of a Copper-Based Oxygen Carrier Prepared by Impregnation for
5 Chemical-Looping Combustion. *Industrial and Engineering Chemistry Research* 43,
6 8168-8177.
- 7 Grace, J.R., 1986. Contacting modes and behaviour classification of gas—solid and other
8 two-phase suspensions. *Canadian Journal of Chemical Engineering* 64, 353-363.
- 9 Gu, H., Shen, L., Xiao, J., Zhang, S., Song, T., 2011. Chemical Looping Combustion of
10 Biomass/Coal with Natural Iron Ore as Oxygen Carrier in a Continuous Reactor. *Energy*
11 *Fuels* 25, 446–455.
- 12 Haider, A., Levenspiel, O., 1989. Drag coefficient and terminal velocity of spherical and
13 nonspherical particles. *Powder Technology* 58, 63-70.
- 14 Harris, A.T., Davidson, J.F., Thorpe, R.B., 2003. Influence of Exit Geometry in Circulating
15 Fluidized-Bed Risers. *AIChE J.* 49, 52-64.
- 16 Johnsson, F., Andersson, S., Leckner, B., 1991. Expansion of a freely bubbling fluidized
17 bed. *Powder Technology* 68(2), 117-123.
- 18 Johnsson, F., Vragar, A., Tikma, T., Leckner, B., 1999. Solids flow pattern in the exit
19 region of a CFB-furnace. Influence of geometry. *Proceedings of the 15th International*
20 *Conference on Fluidized Bed Combustion, Savannah, USA.*
- 21 Kramp, M., Thon, A., Hatge, E.-U., Heinrich, S., Werther, J., 2012. Carbon Stripping – A
22 critical process step in chemical looping combustion of solid fuels. *Chemical*
23 *Engineering Technology* 35, 497-507.
- 24 Levenspiel, O. *Chemical Reaction Engineering*; John Wiley and Sons: New York, 1981.

1 Mahalatkar, K., Kuhlman, J., Huckaby, E.D., O'Brien, T., 2011. CFD simulation of a
2 chemical-looping fuel reactor utilizing solid fuel. *Chemical Engineering Science* 66,
3 3617-3627.

4 Markström, P., Lyngfelt, A., Linderholm, A., 2012. Chemical-Looping Combustion in a
5 100 kW Unit for Solid Fuels. *Proceedings of the 21st Int. Conf. on Fluidized Bed
6 Combustion, Naples (Italy), 4-6 June 2012.*

7 Matthesius, G.A., Morris, R.M., Desai, M.J., 1987. Prediction of the volatile matter in coal
8 from ultimate and proximate analyses. *J. S. Afr. Inst. Min. Metall.* 87(6), 157-161.

9 Palchonok, G., 1998. PhD Thesis, Chalmers University of Technology, Göteborg, Sweden.

10 Pallarès, D., Johnsson, F., 2006. Macroscopic modelling of fluid dynamics in large-scale
11 circulating fluidized beds. *Progress in Energy and Combustion Science* 32(5-6), 539-
12 569.

13 Pillai K.K. The influence of coal type on devolatilization and combustion in fluidized beds.
14 *J. Inst. Energy*, 1981, 54, 142-150.

15 Schöny, G., Pallarès, D., Leion, H., Wolf, J., 2011. Assessment of the scale-up and
16 operational design of the fuel reactor in chemical looping combustion. *Proceedings of
17 the 36th Int. Technical Conference on Clean Coal & Fuel Systems, Clearwater, Florida,
18 USA.*

19 Shen, L., Wu, J., Gao, Z., Xiao, J., 2010. Characterization of chemical looping combustion
20 of coal in a 1 kW_{th} reactor with a nickel-based oxygen carrier. *Combustion and Flame*
21 157, 934-942.

22 Song, T., Shen, L., Xiao, J., Chen, D., Gu, H., Zhang, S., 2012. Nitrogen transfer of fuel-N
23 in chemical looping combustion. *Combustion and Flame* 159, 1286-1295.

- 1 Ströhle, J., Lombarte, A., Orth, M., Epple, B., 2009. Simulation of a Chemical Looping
2 Combustion Process for coal. Proceedings from the 1st Int. Oxyfuel Combustion
3 Conference, Cottbus (Germany).
- 4 Ströhle, J., Orth, M., Epple, B., 2010. Simulation of the fuel reactor of a 1 MWth chemical
5 looping plant for coal. Proceedings of the 1st International Conference on Chemical
6 Looping, Lyon (France), 17-19 March 2010.
- 7 Wen, C.Y., Yu, Y.H., 1966. A Generalized Method for Predicting the Minimum
8 Fluidization Velocity. AIChE J. 12, 610-612.
- 9
10
11